American Heart
Association®

*Learn and Live*sm

Stroke

Acute loss of Aquaporin 4 in relation to vascular injury after stroke

Beth Friedman, Christian Schachtrup, Philbert S. Tsai, Andy Y. Shih, Katerina Akassoglou, David Kleinfeld, and Patrick Lyden
STROKE/2008/523720 VERSION 2

This information is current as of November 21, 2008

Author Disclosures

Beth Friedman: No disclosures

Christian Schachtrup: No disclosures

Philbert S. Tsai: No disclosures

Andy Y. Shih: No disclosures

Katerina Akassoglou:
  Research Grant: Dana Foundation Program in Brain and Immunoimaging, Amount: >= $10,000
                             NIH/NINDS NS052189, Amount: >= $10,000

David Kleinfeld:
  Research Grant: EBOO383201-(NIBIB), Amount: >= $10,000
                             NS058668 (NIH), Amount: >= $10,000

Patrick Lyden:
  Research Grant: NS43300(NIH), Amount: >= $10,000
                             NS052565 (NIH), Amount: >= $10,000
                             VA Merit Grant, Amount: >= $10,000

Acute vascular disruption and Aquaporin 4 loss after stroke

Beth Friedman, Christian Schachtrup, Philbert S. Tsai, Andy Y. Shih, Katerina
Akassoglou, David Kleinfeld and Patrick D. Lyden

From the Department of Neurosciences, Department of Pharmacology, UCSD School of
Medicine, Department of Physics, UCSD, and Veterans Administration Medical
Center, San Diego

Correspondence to:

Patrick D. Lyden, MD, FAAN, FAHA

Stroke Center

200 West Arbor Drive

San Diego, CA 92103-8466

Phone: 619-543-7760

FAX 619-543-7771

plyden@ucsd.edu

ACKNOWLEDGEMENTS and FUNDING

Acute vascular disruption and Aquaporin 4 loss after stroke

Cover Title: Aquaporin 4 loss near disrupted ischemic vessels

Figures: One half-tone, 5 Color

Key Words: Aquaporin 4, Blood Brain Barrier Breakdown, Stroke

ABSTRACT

Background and Purpose: Ischemic protection has been demonstrated by a decrease in stroke-infarct size in transgenic mice with deficient Aquaporin 4 (AQP4) expression. However, it is not known if AQP4 is rapidly reduced during acute stroke in animals with normal AQP4 phenotype, which may provide a potential self-protective mechanism.

Methods: Adult male rats underwent transient occlusion of the middle cerebral artery (tMCAo) for 1 to 8 hours and reperfusion for 30 minutes. Protein and mRNA expression of AQP4 and glial fibrillary acidic protein (GFAP) were determined by Western blot and rtPCR. Fluorescence quantitation was obtained with laser scanning cytometery (LSC) for Cy5-tagged immunoreactivity along with fluorescein signals from pathological uptake of plasma-borne fluorescein-dextran. Cell death was assessed with in vivo Propidium Iodide (PI) nucleus labeling.

Results: In the ischemic hemisphere, patches of fluorescein-dextran label were overlapped with focal loss of AQP4 immunoreactivity after tMCAo of 1 to 8 hours duration. Consistent with focal AQP4 loss, AQP4 protein and mRNA, in striatal homogenates, were not significantly reduced after 8 hour tMCAo. Scan areas, defined by LSC, with high densities of fluorescein-dextran uptake, demonstrated reductions in immunoreactivity for AQP4, but not in IgG or GFAP after tMCAo of 2 hours or longer. Scan areas with low densities of fluorescein-dextran did not lose AQP4. This model of tMCAo resulted in sparse astrocyte cell death as only 1.7 +/- 0.85 % (mean, sd) of DAPI labeled cells were PI and GFAP labeled after 8 hours of tMCAo.

Conclusions: During acute tMCAo, a rapid loss of AQP4 immunoreactivity from viable astrocytes can occur. However, AQP4 loss is spatially selective and occurs primarily in regions of vascular damage.

4

INTRODUCTION

Water balance in the brain is regulated primarily by Aquaporin 4 (AQP4) channels, which are concentrated in perivascular astrocytic end-feet[1] and belong to the multigene family of Aquaporins[2, 3]. Little is known about the kinetics of AQP4 turnover or the physiological basis for maintained AQP4 expression in astrocyte endfeet. The demonstration that reduced[4, 5] or abrogated[6, 7] AQP4 function increases resistance to brain edema arising from stroke in a permanent ischemia model [8-10] has supported the suggestion that AQP4 levels may serve to gate evolving edema after brain injury. Importantly, the protective anti-edema effects observed in transgenic mice are demonstrated in the context of a pre-existing reduction of AQP4 prior to the stroke onset. In normal animals, if AQP4 serves a gating role it would be predicted that its levels should change rapidly in order to impact the earliest phases of stroke-evoked edema.

It is well known that brain injury dysregulates AQP4 channel expression [11, 12] with model-dependent results of both up and down regulation. Brain injury from experimental stroke has been associated with upregulation of tissue AQP4 protein, mRNA and immunoreactivity in both stroke core and infarct in a tMCAo model of 30 minutes occlusion followed by 1 hour of reperfusion in adult mice [13]. Experimental tMCAo in mice has also been linked to fluctuating up and down regulation of AQP4 in a model with 90 minutes of vessel occlusion followed by 1 to 12 hours of reperfusion in adult mice [14]. In this latter study, AQP4 dysregulation converted to a stable and significant reduction

5

after 24 hours of reperfusion in the stroke core and a recovery of AQP4 levels in the penumbra.

It remains unclear if there are conditions that trigger a rapid, possibly, self-protective reduction of brain AQP4 in the acute phase of ischemia, defined here as less than 24 hours post-insult. The perivascular concentration of astrocytic AQP4 suggests a hypothesis that severe vascular injury may interconnect with the regulation of AQP4 channels. An approach to test the hypothesis of a linkage between vascular damage and rapid ischemic changes in AQP4 expression is to determine the effect, on AQP4, of modulating vascular damage through increased duration of ischemic insult [15, 19-21]. The resultant vascular damage that is severe can be monitored on the basis of the presence of pathological endothelial cell permeability to high molecular weight fluorescein-dextran (2 MDa) [15, 16 17 18]. In order to study ischemic alterations in AQP4 that are rapid, brain re-perfusion can be limited to short epochs since even 30 minutes of reperfusion captures acute cytotoxic edema in astrocytes [22] after cardiac arrest. The present study asks then, if a tMCAo model, with varying occlusion-durations and with only 30 minutes of reperfusion, uncovers a capacity for rapid AQP4 loss in ischemic brain regions with severe vascular damage.

6

METHODS

Surgery for tMCAo

All procedures were performed with approval of the VAMC San Diego IACUC. We used 45 male Sprague-Dawley rats (290-305 gm) in this study. Rats were anesthetized with isofluorane; (1-2 % in oxygen: nitrous oxide 30:70) and this was followed by tail-vein injection of 2-MDa fluorescein-dextran (Sigma, St. Louis, MO) (0.3 ml of a 5% (w/v) solution).

For tMCAo, the left common carotid artery was threaded with a 4-0 nylon suture (Ethilon, Animal Health, Baltimore, MD) that was blunted to a diameter between 300 and 310 µm using a microforge (Narishige, East Meadow, NY). The suture was advanced 17.5 to 18.0 mm from the bifurcation point of the external and internal carotid arteries, to block the ostium of the MCA. Occlusion durations varied from 1, 2, 4, or 8 hours and reperfusion time was fixed at 30 minutes. Transcardial perfusion and tissue fixation was performed as previously described[17, 18].

Immunocytochemistry

Brain sections were cut into 50 µm sections and then immunostained[18] with rabbit polyclonal anti-Aquaporin 4 (Chemicon, Temecula, CA or Millipore, Billerica, MA), rabbit polyclonal anti-GFAP (Sigma, St. Louis) or with biotinylated universal secondary antibody for rat IgG staining (Vector, Burlingame, CA). Non-biotinylated primary antibody incubations were followed by incubation in biotinylated anti-rabbit secondary antibody (Vector). For fluorescent localization of biotinylated antibodies, sections were

7

incubated overnight in Cy5-conjugated strepavidin (Jackson Immunoresearch, West

Grove, PA). Fluorescent immunostained sections were washed in PBS and then mounted

on slides and cover-slipped with Pro-Long Antifade mountant (Molecular Probes,

Eugene, OR). Background staining was assessed in sections processed without primary

antibody.

Western Blots

After barbiturate overdose at the end of 8 hours of tMCAo and 30 minutes of reperfusion,

rats were exsanguinated with cold saline and whole striata were subdissected from the

ischemic and contralateral hemispheres and snap frozen in liquid nitrogen (n=4 rats).

Tissue samples were homogenized in a standard lysis buffer [23] that included 1% SDS.

Insoluble material was pelleted in two runs at 14,000 g and resultant lysates were

fractionated on a NuPage 4-12% Bis-Tris gradient gel (Invitrogen, Carlsbad, CA)

followed by transfer to a nylon membrane (Life Sciences, Boston, Mass).

Immunoblotting was performed first with anti AQP4 antibody (1:500 in tween buffered

saline (TBS-T) with 1 % milk). After washing, the membranes were incubated in anti-

rabbit antibody (1:2000 in TBS-T with 5% milk). Immunoreactive protein was

visualized with Western C (BioRad, Hercules, CA) for chemiluminescence. Scanning

densitometry and analysis was obtained with a Versidoc 4000 (BioRad, Hercules, CA).

Blots were stripped twice for reprobing first with anti-GFAP (1:5000 in TBS-T and 5%

milk) and then with anti-beta actin antibody (1:5000 in TBS-T and 5% milk, Sigma-

Aldrich, St Louis, MO). Secondary anti-mouse antibody for GFAP and for beta actin

was provided by Cell Signaling Technologies and used at a concentration of 1:5000 in

8

TBS-T and 5% milk. Lane loading differences were controlled for by normalization to the corresponding actin signals for each sample.

RNA extraction and Real Time RT-PCR

RNA was isolated from frozen tissue samples of ischemic cortex, striatum and contralateral uninjured homologous control tissue after 8 hours of tMCAo using the RNeasy Mini Kit (Qiagen) according to manufacturer's instructions. RNA was reverse transcribed to cDNA using the GeneAmp RNA PCR Core Kit (Applied Biosystems, Foster City, CA) using random hexamer primers. Real time PCR analysis from samples from each rat (n=7) was run in triplicate and performed using the Opticon DNA Engine 2 (MJ Research) and the Power SYBR Green PCR kit (Applied Biosystems) using 1.5 μL of cDNA template in a 25 μL reaction. Results were analyzed with the Opticon 2 Software using the comparative C_T method, as described[24]. Data were expressed as $2^{-\Delta\Delta C_T}$ for the experimental gene of interest normalized against the housekeeping gene GAPDH and presented as fold change *vs.* contralateral control samples. The primers were designed using the Primer Express software (Applied Biosystems) following the guidelines suggested in the Primer Express applications-based primer design manual. The following primers were used:

GFAP: Fwd 5' GCGGCTCTGAGAGAGATTCG 3'

                   Rev 5' TGCAAACTTGGACCGATACCA 3'

Aquaporin4:   Fwd 5' TGCTGGCAGGTGCACTTTAC 3'

                   Rev 5' GCTGTGCAGCTTTGCTGAAG 3'

9

GAPDH: Fwd 5' CTCTACCCACGGCAAGTTCAA 3'

                   Rev 5' CGCTCCTGGAAGATGGTGAT 3'

Imaging and Quantitative Analysis

Digitized fluorescent images were acquired with an Olympus BX50 Microscope fitted

with a CompuCyte[TM] laser scanning cytometry (LSC) acquisition system (Olympus of

America, Cambridge, MA). Fluorescein fluorescence, from excitation with a focused

argon laser (488 nm), was collected through an emission filter with a bandwidth of

530 ± 30 nm. Cy5 fluorescence, from excitation with a focused helium-neon laser

(633 nm) was collected through an emission filter with a bandwidth of 675 ± 50 nm.

Fluorescein and Cy5 gates were set for background levels that were determined from

negative control tissue sections. Section fluorescence was digitized from 40 µm diameter

scan areas that were tiled across the whole section (e.g. Fig 4A2 and 4A3). The

thresholded and integrated fluorescence signal intensities for both fluorescein and Cy5

determined whether a particular scan area was classified as backround, or single or

double labeled. This is illustrated by the scattegrams created by the Wincyte[TM] software

(Fig. 4A4). For example, the scattergram in Fig. 4A4 provides a frequency of double

labeled scan areas (1047, or 3% of the total number of scan areas) from the digitization of

the section illustrated in Figures 4A1 and 4A3; then, a whole section double label index

was calculated from the ratio of double labeled scan areas (upper right quadrant) to the

number of all scan areas with dextran signal (sum of upper and lower right quadrants: Fig

4A4) in order to normalize the double labeling frequency. Laser scanning cytometry was

10

also used to compare total AQP4 in operator-defined sub-regions of interest that typically covered 300 scan areas. The operator-defined sub-regions were placed in areas high levels of fluorescein-dextran label and in areas with low levels of fluorescein-dextran label (boxes in Figs. 4A3). For striatal analyses, data was obtained from 2 high label subregions and from 2 to 4 low label subregions/per section in 1 to 2 sections per rat. In ischemic neocortex, the analysis of the AQP4 staining was restricted to 8 hours of tMCAo cases and included selection of 1 high leakage subregion and 1 to 2 low leakage subregions in 1 to 2 sections per rat. Brain sections selected for striatal or neocortex analysis originated from levels that spanned from 0.1 mm anterior to -0.3 mm posterior to Bregma[25].

In vivo Propidium Iodide Labeling

Rats were subjected to 8 hours of tMCAo (n=3) and propidium iodide (0.3 ml of a 2mg/ml solution) was injected via tail vein for the last 2 hours of occlusion (n=2) or for the last 4 hours of occlusion (n=1). All rats were reperfused for 30 minutes and then killed with a barbiturate overdose followed by transcardial perfusion with saline and then buffered paraformaldehyde fixative. The brains were removed, cryoprotected in 30% sucrose and cryostat sectioned at 15 μm. Immunostaining for GFAP was performed after antigen retrieval [17] with visualization either with cy5-avidin or with use of Alexa-conjuated GFAP primary antibody (Invitrogen, Carlsbad, CA). Slides were coverslipped with Prolong-Gold[TM] mountant containining DAPI for nuclear visualization (Invitrogen, Carlsbad, CA). Data was collected on an Olympus scanning confocal microscope with a 60 X oil objective. For each case 15 to 20 fields were examined in each of two sections

11

from PI positive regions, identified in ischemic striatum at lower magnification (10x objective), for a total count of 1848 DAPI positive cells.

Two-Photon Microscopy

Fluorescent images of 2-MDa fluorescein-dextran leakage and of the Cy5 tagged AQP4 fluorescence in 50 μm thick sections were acquired with a two-photon microscope of local design[26]. Volume rendered images of the vessel fluorescence was performed with using VOX2 (public domain software) and with MatLab (The Mathworks, Natick, MA). Spectral separation of these images was performed by subtracting the cross-over fluorescein signal from the image observed in the Cy5 channel.

Statistical Analyses

The double label index (double-positive counts normalized to total fluorescein-dextran in individual sections) was assessed for differences as a function of occlusion duration using one-way ANOVA. To assess the significance of differences between the high and low dextran subregions over different occlusion durations, one-way ANOVA was used with Tukey's procedure for testing differences post-hoc. Plotted immunocytochemical data was expressed as mean±2 SE (standard errors). The paired t-test was used to assess the significance of differences of mean values, in neocortex, in the total fluorescence in high and low leakage subregions after 8 hours of tMCAo. Differences between means of GFAP and AQP4 mRNA in cortex and striatum relative to the contralateral side were assessed by ANOVA. Data from Western blots and rtPCR were plotted as mean±1 SE.

12

RESULTS

Acute tMCAo of one hour resulted in patchy reductions in AQP4 immunoreactivity

(Fig. 1). Patches of tissue marked by pathological uptake of 2MDa fluorescein-dextran

overlapped regions with AQP4 staining deficiencies (Fig.1). There was negligible

fluorescein-dextran uptake on the contralateral side of the brain, supplied by the non-

occluded middle cerebral artery (Fig. 1). A macroscopic spatial correspondence between

AQP4 immunostaining deficiencies and fluorescein-dextran tagged tissue uptake was

further observed after 2, 4, and 8 hours of tMCAo (Fig. 2). Regions of reduced AQP4

staining and of emerging fluorescein-dextran labeling expanded with occlusion duration,

especially in the striatum. After 8 hours tMCAo, patchy AQP4 reduction and patches of

dextran labeling were also distributed in the ischemic neocortex (Fig. 2 and see

supplemental Figure 1). These data provide qualitative support for a rapid dysregulation

of brain AQP4 after stroke.

To determine if the macroscopic reduction in AQP4 immunostaining reflects an overall

loss of AQP4 protein, Western blots for AQP4 immunoreactivity were performed on

tissue lysates from whole striata. The analyses were restricted to cases with 8 hours of

tMCAo, as this occlusion duration was associated with the greatest macroscopic loss of

AQP4 immunoreactivity. On average, no significant loss of AQP4 protein was detected

in ischemic striata (Fig. 3A). Similarly, rtPCR of AQP4 at 8 hours demonstrates no

significant change in AQP4 mRNA expression (Fig. 3B). However, GFAP mRNA is

significantly increased in the ischemic striata (Fig. 3B and see Supplemental Figure 2).

13

This lack of significant change in AQP4 protein or mRNA in tissue homogenates may arise from a micro-heterogeneity of loss of AQP4. Thus, high resolution microscopy of the ischemic striatum, after 8 hours of tMCAo, demonstrated individual fluorescein-dextran labeled vessels which lack perivascular AQP4 as well as other vessels which showed persistent perivascular AQP4 label (Fig. 3C). This micro-heterogeneity limits quantitation of acute changes in AQP4, after stroke, to methods that do not blur focal changes.

To test if stroke-induced fluorescein-dextran labeling provides a tool to stratify spatially micro-heterogeneous changes in AQP4 expression, we segmented immunoreactivity according to the presence of concomitant uptake and tissue-labeling by high molecular weight fluorescein-dextran. Laser scanning cytometry analysis of whole brain sections (Fig. 4A1-4A5) was used to probe scan areas of 40 μm diameter. These scan areas were rastered across whole brain sections (Fig. 4A2). Consideration of the number of scan areas with fluorescein-dextran label in whole brain sections demonstrates a significant increase in number after 4 or 8 hours of tMCAo relative to 1 hour tMCAo (Fig. 4A5), consistent with the macroscopic data illustrated in Fig. 2.

The fluorescein-dextran positive scan areas were further assessed for the presence or absence of Cy5-tagged immunolabel. This was quantified as a double-label index (Fig. 4F) which reflects a section by section normalization of the number of double-labeled scan areas to the total number of fluorescein-dextran scan areas per section. The double-label index of scan areas with both AQP4 (Cy5) and fluorescein-dextran label after 2

14

hours tMCAo (57%±14%, mean±2 SE) was significantly less than this index after 1 hour

tMCAo (84%±8%; p<0.02 for 1 hour versus 2 hour tMCAo, ANOVA with Dunnett's

procedure). Further AQP4 reductions were observed with longer tMCAo (p<0.001 for 1

hour versus 4 hour or 8 hour tMCAo). However, even at 8 hour tMCAo, double-labeled

scan areas were present, consistent with high resolution micrococpic examination (see Fig.

3C). These data indicate that stratification of AQP4 staining according to proximity to

stroke-induced high molecular weight fluorescein-dextran uptake permits quantitation of

AQP4 staining loss in response to acute stroke.

The double-label index for immunoreactivity to biotinylated IgG was determined as a

technical control. This allowed evaluation of whether the reduction of the AQP4 double-

label index represented a non-specific effect of ischemic brain swelling since swelling

alone could reduce the density of AQP4 positive scan areas. As focal cerebral ischemia

triggers leakage to endogenous blood-borne molecules such as IgG, we predicted that

counting regions labeled with fluorescein-dextran should also contain IgG

immunoreactivity. Immunoreactivity to IgG, reported by Cy5, resulted in label of brain

parenchyma in areas with blood vessels that were marked by fluorescein-dextran uptake

(Figs. 4D1, 4D2, 4F). However, in contrast to AQP4, the double-label index for IgG and

fluorescein-dextran showed no significant change with increased tMCAo duration (Fig.

4F). The stability of the IgG and fluorescein-dextran double-labeling index indicates that

dextran leakage and IgG extravasation increase in parallel with longer durations of

tMCAo. Thus, the reduction in AQP4 immunoreactivity, proximate to uptake of high

15

molecular weight fluorescein-dextran by hyperpermeable vessels, is not a result of brain swelling.

To determine whether the decline in the AQP4 double-label index generalized to an independent marker for astrocytes, we determined the double-label index for GFAP (Figs. 4E1, 4E2). GFAP staining intensity was especially dense in regions of fluorescein-dextran label and also near the lateral ventricle (Figs. 4E1, 4E2). The double labeling index for GFAP and fluorescein-dextran did not change significantly with tMCAo duration (Fig. 4F). Therefore, the expansion of dextran labeling over increasing occlusion duration occurred among populations of astrocytes with simultaneously increased GFAP staining and reduced AQP4 immunoreactivity.

Ischemic regions with low levels of dextran leakage showed less dysregulation of AQP4 immunoreactivity. This is illustrated in Figure 5A which shows similar levels of AQP4 staining in the nonischemic striatum and in the ischemic striatum in fields that span across areas with high to low levels of dextran leakage. Immunoreactivity for AQP4 in areas with low levels of dextran leakage was qualitatively similar in ischemic and contralateral striatum after tMCAo of 1 or 4 hours duration. After 8 hours of tMCAo, AQP4 immunoreactivity was more heterogeneous in ischemic areas with low levels of dextran, as there were patches of increased and reduced staining (Fig. 5A).

In order to test the qualitative impression of an apparent stability in the AQP4 immunoreactivity in ischemic regions with low levels of fluorescein-dextran leakage,

16

total AQP4 staining density was determined in operator-defined subregions that were segmented according to fluorescein-dextran leakage. The analyzed regions typically encompassed 300 scan areas (for examples of operator-defined subregions see boxes in the fluorescein-dextran rich area on the ischemic side and in the fluorescein-dextran poor area on the contralateral side of the digitized section in Fig. 4A3). Scanned subregions with high or low densities of fluorescein-dextran label were identified for all durations of tMCAo (Fig. 5B). The AQP4 staining density in such subregions was also measured (Fig. 5C). In subregrions with low fluorescein-dextran the total Aquaporin 4 immunoreactivity showed no significant change over increasing durations of occlusion (Fig. 5C). In contrast, in subregions with a high density of fluorescein-dextran the total AQP4 immunoreactivity declined with increasing occlusion duration (Fig. 5C, white bars) (ANOVA was used with Tukey's procedure for post-hoc comparisons, F=3.78, p=0.018).

Aquaporin 4 staining was additionally disrupted in ischemic neocortex after 8 hours of tMCAo (Fig. 2 and see supplementary Fig. 1). Subregion quantitation of AQP4 staining density, in 8 hour tMCAo ischemic neocortex, showed significant reductions of AQP4 in high–dextran leakage subregions relative to low-leakage regions (9.2±3% vs 17.4±1.8%, mean ± SEM; n=5 rats; t test, p=0.033). Thus regions with low uptake of high molecular weight fluorescein-dextran in ischemic neocortex, ischemic striatum and contralateral striatum share the characteristic of resistance to ischemic loss of AQP4 immunoreactivity after 8 hours of tMCAo.

The rapidity and selectivity of staining loss for AQP4 but not GFAP after acute tMCAo suggests that the loss of AQP4 staining may be a dynamic response in viable but ischemic astrocytes. The question of astrocyte viability, especially after 8 hours of tMCAo, prompted further evaluation of the ischemic striatum to search for early infarction, as defined by cell death. To quantitatively assess striatal infarction, the integrity of cell nuclei labeled by DAPI (4', 6-diamidino-2-phenylindole) was assayed by their prior uptake of circulating propidium iodide (PI) in vivo (Fig.6). Such in vivo uptake of propidium iodide has previously [27] been shown to label dying cells after brain injury. After 8 hours tMCAo, the PI labeling index in the ischemic striatum of DAPI labeled nuclei was less than 10 % (7.6%+/- 2.7%; mean, sd) (Fig. 6C). Cells tripled labeled with GFAP, DAPI and PI accounted for 1.7 +/- 0.85% (mean, sd) of all DAPI labeled cells. The low incidence of PI nuclear labeling suggests that this model of acute stroke coincides with very early striatal infaction. Thus the loss of AQP4 staining observed after 8 hours of tMCAo is not explained by widespread stroke-induced astrocyte cell death.

18

DISCUSSION

We sought to determine whether ischemic dysregulation of astrocytic AQP4 could occur

rapidly in response to experimental stroke in animals with normal AQP4 phenotype.

Immunocytochemical data provided qualitative evidence that even 1 hour of tMCAo results

in patchy staining loss of AQP4; the heterogeneity of this astrocyte response is

corroborated by the absence of detectible reductions of AQP4 protein or mRNA in whole

striatal homegenates. Early focal reductions of AQP4, in regions with pathological uptake

of fluorescein-dextran were quantified with laser scanning cytometry, between 1 and 2

hours of tMCAo. Increased duration of tMCAo, to occlusions of 4 hours, resulted in both

an expansion of vascular damage, as evidenced by the spread in high molecular weight

fluorescein-dextran uptake, and also in a further reduction in the AQP4-fluorescein-dextran

double labeling index. The fall in the double-labeling index was selective for AQP4

immunoreactivity since the double-label index for IgG and GFAP remained stable with

increased occlusion duration. The decline in AQP4 was also selective for scan areas with

high levels of fluorescein-dextran tissue label since AQP4 was not significantly altered in

clusters of scan areas with sparse fluorescein-dextran label. Taken together our findings

suggest that stroke can cause rapid losses in AQP4 staining in those ischemic astrocytes

where ischemic injury has been sufficiently severe to allow pathological passage of high

molecular weight fluorescein-dextran (2megadalton) across ischemic vasculature.

Our demonstration of rapid changes in AQP4 during the acute phase of stroke extends

previous experimental studies[14] and human pathology data[28], where AQP4 loss has been

19

observed after longer post-stroke survival periods. The chronic AQP4 loss observed in human stroke infarcts has been ascribed to associated astrocyte cell death. However, in light of the present study it is also possible that the persistent loss of AQP4 actually originated as an early rapid response of astrocytes during acute injury, as our data indicates that AQP4 loss occurs in the face of retained GFAP expression and in advance of widespread ischemic death. The notion that AQP4 loss represents an active rapid physiological response in viable astrocytes is supported by recent work documenting a reversibility of AQP4 loss in the stroke penumbra of adult mice[14]. In addition, the seminal observations of the extraordinarily rapid disappearance of membrane particle assemblies, later identified as astrocytic perivascular AQP4 channels, in response to circulatory arrest [22] further argues that the loss of AQP4 after ischemic stroke can represent an active astrocyte response.

The results should be interpreted in light of the limitation of examination of tMCAo occlusions of 1 hour durations or longer. The one hour occlusion time was chosen because shorter occlusion durations failed to yield consistent labeling of ischemic vasculature or parenchyma by circulating high molecular weight fluorescein-dextran and our LSC stratification depends on the presence of fluorescein-dextran labeling of scan areas. Thus hyperacute effects of ischemia on AQP4 dysregulation cannot be inferred from the present acute study. This limitation speaks to the need for future experiments in which AQP4 expression changes are visualized in real-time in relation to an ischemic insult, possibly in mice that could be engineered to express GFP–tagged AQP4.

20

Our data contrasts with other experimental models in which blood brain barrier breakdown has been shown to provoke acute upregulation of AQP4. Sudden blood brain barrier breakdown and inflammation from intraparenchymal injection of lipopolysaccharide (LPS)[31] into the substantia nigra of female rats results in significant increases in the number of AQP4 mRNA positive cells after 6 hours after injury. Furthermore, in vitro studies[32] demonstrate that administration of IL-1, a mediator of edema after ischemia, up-regulates AQP4 mRNA in rat astrocytes *in vitro* and consequent to intracerebroventricular administration in rat brain *in vivo*. This supports a role for vascular leakage as a potential mediator of up-regulation of AQP4 after brain injury. On the other hand, LPS injection into the chick optic tectum results in reductions of AQP4 immuno-reactive protein in perivascular astrocytic endfeet[33]. Experimental studies with stroke models in mice have also yielded contradictory results concerning the effects of stroke on the regulation of AQP4. For example, mice that were subjected to 30 minute occlusion duration tMCAo demonstrated significant increases in immunoreactivity in both the ischemic core and in the surrounding penumbra at 1 and 48 hours of reperfusion[13]. However, a separate study of stroke in mice[14] demonstrated reductions in AQP4 immunoreactivity in perivascular astrocytic glial endfeet in ischemic striatum after 24 hour of reperfusion. Of interest, the MCA occlusions in the latter study that resulted in reductions in AQP4 immunoreactivity, were 1 hour longer than the MCA occlusions that resulted in stroke-evoked increases in AQP4 levels. Thus the loss of AQP4 after stroke may require a critical duration or severity of ischemic injury.

21

Little is known about the molecular mechanisms that regulate expression of AQP4 in normal or in injured astrocytes. AQP4 promoter regions have been identified with binding activity for transcription factors that are up-regulated by ischemia and hypoxia (reviewed in Simard et al[34]). Non-disease conditions such as pregnancy also up-regulate the expression of astrocyte AQP4[35]. On the other hand other types of brain injury that do not involve widespread ischemia, such as hypertensive encephalopathy have been shown to result in reductions in perivascular AQP4 immunoreactivity[29]. Regulation of AQP4 mRNA at subacute (48 hour survival times) has been linked[36] to antecedent alterations in levels of targeted mircroRNA sequences. However there are also precedents for a role for channel regulation processes that are independent of changes at the level of transcription; for example, AQP2 surface-expression and function in the kidney is rapidly inactivated by channel ubiquitination followed by endocytosis[37] in response to channel phosphorylation. Furthermore, endocytotic regulation of AQP4 channels expression can be extremely rapid as histamine stimulation provokes rapid AQP4 internalization and reduced water transport as early as 20 minutes after stimulation[38] in a gastric parietal cell line. In conclusion, the demonstration of rapid but selective loss of AQP4 from rat brain astrocytes suggests that brain astrocytes may possess the cellular machinery for a self-protective response to early ischemia; however, the localization of this effect to regions that are supplied by blood vessels that have been severely damaged by stroke may indicate that there is a injury threshold for this effect.

22

FIGURE LEGENDS

Figure 1.

Immunostaining of AQP4 after 1 hour of tMCAo. Panels on left are scans of a single section imaged for Cy5-AQP4 immunoreactivity (top left), for pathological fluorescein-dextran uptake (middle left); the bottom left panel shows the merged image. Middle panels are views of the section that are converted to grey scale and inverted for clarity. Right panels show areas at arrows at higher magnification. The pale area that lacks Aquaporin 4 staining overlies a dense patch of high-molecular weight fluorescein dextran uptake.

Figure 2.

Whole brain sections from cases with tMCAo of 1, 2, 4 or 8 hours duration imaged for AQP4 immunoreactivity (left panels) and for fluorescein-dextran uptake (right panels). The striatum in the ischemic hemisphere shows pale areas with reduced AQP4. Fluorescein images demonstrate overlapping areas with high molecular weight fluorescein-dextran uptake. In the ischemic neocortex, after 8 hours of tMCAo, periodic discontinuities emerge in the AQP4 immunoreactivity along with patches of fluorescein-dextran leakage. The contralateral cortex retains a normal, continuous AQP4 staining pattern. Scale bar = 1mm.

23

Figure 3.

Average AQP4 mRNA and protein expression levels in homogenates of whole ischemic
and contralateral striata after 8 hours of tMCAo as determined from Western blot and
rtPCR analyses.

(A) Quantitation of AQP4 and GFAP protein by Western blot from whole ischemic
striata (I) and contralateral striata (C) after 8 hours tMCAo (n=4). Each lane was loaded
with 30 µg of protein. Loading variations were controlled for by normalization to actin
levels in each sample. Bars show mean +/- SEM. There were no significant changes in
AQP4 or GFAP protein levels in ischemic striata relative to the contralateral side.

(B) Quantitation of AQP4 and GFAP mRNA by rtPCR of whole ischemic and
contralateral striata and cortices after 8 hours tMCAo (n=7). Gene expression data was
normalized to GAPDH and presented as fold change (mean ± SE) versus the contralateral
striata or cortex. The differences in bar height were not significant for AQP4 (ns).
GFAP mRNA in ischemic striata and cortices was significantly greater than levels on the
contralateral side (ANOVA, $p<0.005$).

(C) High resolution images of fluorescein-dextran labeling (green) and perivascular
AQP4 staining (red) in a microvessel after tMCAo of 8 hours. Rotated view (labeled X-
Z) shows vessel in cross-section; note intensely fluorescent vessel walls labeled with
fluorescein-dextran uptake, unlabelled vessel lumen and perivascular AQP4. Images
illustrate heterogeneity of perivascular AQP4 expression in single sections of striata.

24

Figure 4.

The use of laser scanning cytometry (LSC) to compare of the effects of increased

occlusion duration on the frequency of scan areas that are co-labelled by fluorescein-

dextran and immunoreactivity to AQP4, IgG or GFAP.

(A1 and A2) illustrate a brain section that shows fluorescein-dextran labeling in ischemic

hemisphere after 8 hours of tMCAo in a photomicrograph (A1) and in a companion LSC-

generated digitization of this section (A2).

(A3) Example of 40 µm-diameter scan areas used to quantify fluorescence. This panel

illustrates positive scan areas which result from vascular uptake of high molecular weight

fluorescein-dextran from a case after 2 hours of tMCAo.

(A4) LSC generated scattergram with data from scan areas rastered across an entire

section. Each quadrant provides the per cent area for 1 of 4 different types of counts: 1.

The upper left quadrant demonstrates single-labeled Cy5 immunoreactivity; 2. The upper

right quadrant demonstrates counting regions that are double positive for fluorescein-

dextran and Cy5; 3. The lower right quadrant demonstrates counting regions single-

labeled with fluorescein-dextran; 4. The lower left quadrant demonstrates counting

regions with only background levels of signal. The double labeling indices for whole

sections shown in graphs in panel (F) were determined from the per cent of total scan

areas per section that are double positive (in the upper right quadrant) and this value is

then normalized to the summed percent of scan areas with fluorescein-dextran label

(obtained from the upper and lower right quadrants).

(A5) Changes in the density of scan areas with fluorescein-dextran label as a function of

occlusion duration of tMCAo. The number of cases that were assayed at individual

25

occlusion durations was: 1 hour tMCAo, n=5; 2 hour tMCAo, n=6; 4 hour tMCAo n=5; 8 hour tMCAo, n=5. Different sections from each brain, at the level of the anterior commissure, were immunostained with AQP4, IgG, and GFAP. From 1 to 2 sections per stained series were LSC assayed for fluorescein-dextran uptake so that the dextran density index shown in panel (A5) represents an average value across 16 to 19 sections per occlusion duration. The dextran density index is the total number of fluorescein-dextran labeled scan areas divided by the total number of scan areas for that brain section. The areal density of fluorescein-dextran uptake increases significantly with occlusion duration (1 vs 4 hours p< 0.05 and 1 vs 8 hours; p<0.001: ANOVA followed by Tukey's test).

(B) Images of immunostaining merged with fluorescein-dextran label in a 50 μm section from one brain after 2 hours of tMCAo. Sections are within a 1 mm thick block.

(B1) Fluorescein-dextran uptake concentrates among segments of microvessels.

(B2) Higher magnification of inset (white box in B1) shows heterogeneity in label intensity in affected vessels of varying caliber.

(C1) Fluorescent merged image of fluorescein-dextran labeled vasculature (green with yellow-green borders) and AQP4 immunoreactivity (red).

(C2) The inset panel shows overlap of vessels marked by fluorescein-dextran uptake within the vessel (green), and by perivascular AQP4 which is yellow near vessels with fluorescein-dextran leakage or red near vessels that are unlabelled by fluorescein-dextran.

(D1) Merged images of fluorescein-dextran labeled vasculature and IgG leakage (red).

(D2) High magnification of merged image demonstrates nearly complete overlap of fluorescein-dextran fluorescence and Cy5-IgG immunoreactivity (yellow from

26

intravascular fluorescein-dextran and IgG). This section is the same section shown in panels B1 and B2 where the fluorescein-dextran fluorescence appears green. Fluorescein-dextran labeled vessels are also surrounded by Cy5-IgG immunoreactivity, consistent with widespread extravasation of IgG after stroke.

(E1) Fluorescent merged image of fluorescein-dextran labeled vasculature (green) and GFAP immunoreactivity (red).

(E2) Fluorescein- dextran-labeled vasculature intersperses with densely stained GFAP stained astrocytes.

(F) Comparison of the effect of increased occlusion duration on co-labeling with fluorescein-dextran and Cy5 labelled immunoreactivity for AQP4, IgG and GFAP in scan areas rastered across whole brain sections. Relative to the AQP4 double label index after 1 hour of tMCAo, the AQP4 double-label index was significantly reduced after 2, 4, and 8 hours of tMCAo. In contrast, the IgG and GFAP double-label index did not decline after 1 hour of tMCAo. Double-label index data was obtained from 5 to 6 sections (1-2 sections per rat brain) for each occlusion-duration.

Figure 5.

Immunoreactivity of AQP4 as quantified with LSC, in brain areas with minimal uptake of high molecular weight fluorescein–dextran.

(A) Regions with low levels of fluorescein-dextran signal on the ischemic and contralateral sides of the brain show similar levels of AQP4 immunoreactivity after 1 and 4 hours of tMCAo. Larger vessels in these images appear more densely stained then network of microvessels. At 8 hours of tMCAo regions of low fluorescein-dextran are

27

more heterogeneously stained and exhibit areas of reduced and elevated AQP4 immunoreactivity relative to the contralateral side. The ovoid structures in 8 hour images are clusters of myelinated fibers which typically show little AQP4 immunoreactivity (e.g. also illustrated by sparsely stained white matter tracts in Figure 2).

(B) Laser scanning cytometry (LSC) quantitation of tissue fluorescence from rasterized scans of operator-defined subregions that encompass about 300 scan areas in regions with low or high levels of fluorescein-dextran signal (see methods). The y axis plots the number of scan areas with fluorescein signal divided by the total number of scan areas for that subregion. Subregions of low and high levels of fluorescein dextran were operator-segmented within brain sections. Data for total fluorescence measures was taken from 5 to 6 sections per occlusion duration (1-2 sections per rat brain).

(C) Quantitation of AQP4 Cy5 signal in operator-defined subregions. The y axis plots the number of scan areas with Cy5 label divided by the total number of scan areas of that subregion. There was a progressive loss of AQP4 staining in the region of high leakage, but not in the regions of low leakage within the ischemic or contralateral hemispheres (repeated measures ANOVA, p<0.02).

Figure 6.

Cell death induced by acute stroke was identified by in vivo uptake of circulating Propidium Iodide. A series of images of one field are shown. Panels A1 and A2 show DAPI stained nuclei in ischemic striatum (in A1) and the corresponding distribution of PI nuclear uptake consequent to loss of plasmalemma permeability barriers in dying cells (in

28

A2). Merged image (white arrowhead) shows white halo at site of overlap of DAPI and PI.

Panels B1 and B2 show the GFAP immunoreactivity of a cell co-labeled by PI (arrowhead) and in an adjacent PI negative cell (double arrow).

(C) Pie chart of proportion of cells (DAPI positive) which are co-labeled with propidium iodide or GFAP. The blow-up chart on the right delineates the proportion of propidium iodide positive cells which are co-labeled by GFAP (in tan sector). Data are based on 2 sections per rat brain (n=3) in fields imaged at 60x in the ischemic striatum. The number of DAPI cells counted per rat brain was 594, 566 and 678.

REFERENCES

1. Nielsen S, Nagelhus EA, Amiry-Moghaddam M, Bourque C, Agre P, Ottersen OP. Specialized membrane domains for water transport in glial cells: High-resolution immunogold cytochemistry of aquaporin-4 in rat brain. *J Neurosci*. 1997;17:171-180

2. Agre P, King LS, Yasui M, Guggino WB, Ottersen OP, Fujiyoshi Y, Engel A, Nielsen S. Aquaporin water channels--from atomic structure to clinical medicine. *J Physiol*. 2002;542:3-16

3. Jung JS, Bhat RV, Preston GM, Guggino WB, Baraban JM, Agre P. Molecular characterization of an aquaporin cdna from brain: Candidate osmoreceptor and regulator of water balance. *Proc Natl Acad Sci U S A*. 1994;91:13052-13056

4. Neely JD, Amiry-Moghaddam M, Ottersen OP, Froehner SC, Agre P, Adams ME. Syntrophin-dependent expression and localization of aquaporin-4 water channel protein. *Proc Natl Acad Sci U S A*. 2001;98:14108-14113

5. Amiry-Moghaddam M, Xue R, Haug FM, Neely JD, Bhardwaj A, Agre P, Adams ME, Froehner SC, Mori S, Ottersen OP. Alpha-syntrophin deletion removes the perivascular but not endothelial pool of aquaporin-4 at the blood-brain barrier and delays the development of brain edema in an experimental model of acute hyponatremia. *Faseb J*. 2004;18:542-544

6. Ma T, Yang B, Gillespie A, Carlson EJ, Epstein CJ, Verkman AS. Generation and phenotype of a transgenic knockout mouse lacking the mercurial-insensitive water channel aquaporin-4. *J Clin Invest*. 1997;100:957-962

7. Papadopoulos MC, Verkman AS. Aquaporin-4 and brain edema. *Pediatr Nephrol*. 2007;22:778-784

8. Manley GT, Fujimura M, Ma T, Noshita N, Filiz F, Bollen AW, Chan P, Verkman AS. Aquaporin-4 deletion in mice reduces brain edema after acute water intoxication and ischemic stroke. *Nat Med*. 2000;6:159-163

9. Manley GT, Binder DK, Papadopoulos MC, Verkman AS. New insights into water transport and edema in the central nervous system from phenotype analysis of aquaporin-4 null mice. *Neuroscience*. 2004;129:983-991

10. Amiry-Moghaddam M, Otsuka T, Hurn PD, Traystman RJ, Haug FM, Froehner SC, Adams ME, Neely JD, Agre P, Ottersen OP, Bhardwaj A. An alpha-syntrophin-dependent pool of aqp4 in astroglial end-feet confers bidirectional water flow between blood and brain. *Proc Natl Acad Sci U S A*. 2003;100:2106-2111

11. Vizuete ML, Venero JL, Vargas C, Ilundain AA, Echevarria M, Machado A, Cano J. Differential upregulation of aquaporin-4 mrna expression in reactive astrocytes after brain injury: Potential role in brain edema. *Neurobiol Dis*. 1999;6:245-258

12. Ke C, Poon WS, Ng HK, Pang JC, Chan Y. Heterogeneous responses of aquaporin-4 in oedema formation in a replicated severe traumatic brain injury model in rats. *Neurosci Lett*. 2001;301:21-24

13. Ribeiro Mde C, Hirt L, Bogousslavsky J, Regli L, Badaut J. Time course of aquaporin expression after transient focal cerebral ischemia in mice. *J Neurosci Res*. 2006;83:1231-1240

14. Frydenlund DS, Bhardwaj A, Otsuka T, Mylonakou MN, Yasumura T, Davidson KG, Zeynalov E, Skare O, Laake P, Haug FM, Rash JE, Agre P, Ottersen OP, Amiry-Moghaddam M. Temporary loss of perivascular aquaporin-4 in neocortex after transient middle cerebral artery occlusion in mice. *Proc Natl Acad Sci U S A*. 2006;103:13532-13536

15. Nagaraja TN, Keenan KA, Brown SL, Fenstermacher JD, Knight RA. Relative distribution of plasma flow markers and red blood cells across bbb openings in acute cerebral ischemia. *Neurol Res*. 2007;29:78-80

16. Nagaraja TN, Keenan KA, Fenstermacher JD, Knight RA. Acute leakage patterns of fluorescent plasma flow markers after transient focal cerebral ischemia suggest large openings in blood-brain barrier. *Microcirculation*. 2008;15:1-14

17. Nishimura N, Schaffer CB, Friedman B, Tsai PS, Lyden PD, Kleinfeld D. Targeted insult to subsurface cortical blood vessels using ultrashort laser pulses: Three models of stroke. *Nat Methods*. 2006;3:99-108

18. Schaffer CB, Friedman B, Nishimura N, Schroeder LF, Tsai PS, Ebner FF, Lyden PD, Kleinfeld D. Two-photon imaging of cortical surface microvessels reveals a robust redistribution in blood flow after vascular occlusion. *PLoS Biol*. 2006;4:e22

19. Neumann-Haefelin T, Kastrup A, de Crespigny A, Yenari MA, Ringer T, Sun GH, Moseley ME. Serial mri after transient focal cerebral ischemia in rats: Dynamics of tissue injury, blood-brain barrier damage, and edema formation. *Stroke*. 2000;31:1965-1972; discussion 1972-1963

20. Matsumoto K, Lo EH, Pierce AR, Wei H, Garrido L, Kowall NW. Role of vasogenic edema and tissue cavitation in ischemic evolution on diffusion-weighted imaging: Comparison with multiparameter mr and immunohistochemistry. *AJNR Am J Neuroradiol*. 1995;16:1107-1115

21. Barber PA, Hoyte L, Kirk D, Foniok T, Buchan A, Tuor U. Early t1- and t2-weighted mri signatures of transient and permanent middle cerebral artery occlusion in a murine stroke model studied at 9.4t. *Neurosci Lett*. 2005;388:54-59

22. Landis DM, Reese TS. Astrocyte membrane structure: Changes after circulatory arrest. *J Cell Biol*. 1981;88:660-663

23. You X, Boyle DL, Hammaker D, Firestein GS. Puma-mediated apoptosis in fibroblast-like synoviocytes does not require p53. *Arthritis Res Ther*. 2006;8:R157

24. Livak KJ, Schmittgen TD. Analysis of relative gene expression data using real-time quantitative pcr and the 2(-delta delta c(t)) method. *Methods*. 2001;25:402-408

25. Paxinos G, Watson C, Pennisi M, Topple A. Bregma, lambda and the interaural midpoint in stereotaxic surgery with rats of different sex, strain and weight. *J Neurosci Methods*. 1985;13:139-143

26. Tsai PS, Friedman B, Ifarraguerri AI, Thompson BD, Lev-Ram V, Schaffer CB, Xiong Q, Tsien RY, Squier JA, Kleinfeld D. All-optical histology using ultrashort laser pulses. *Neuron*. 2003;39:27-41

27. Whalen MJ, Dalkara T, You Z, Qiu J, Bermpohl D, Mehta N, Suter B, Bhide PG, Lo EH, Ericsson M, Moskowitz MA. Acute plasmalemma permeability and protracted clearance of injured cells after controlled cortical impact in mice. *J Cereb Blood Flow Metab*. 2008;28:490-505

28. Aoki K, Uchihara T, Tsuchiya K, Nakamura A, Ikeda K, Wakayama Y. Enhanced expression of aquaporin 4 in human brain with infarction. *Acta Neuropathol (Berl)*. 2003;106:121-124

29. Qi X, Mochly-Rosen D. The pkc{delta} -abl complex communicates er stress to the mitochondria - an essential step in subsequent apoptosis. *J Cell Sci*. 2008;121:804-813

30. Rash JE, Yasumura T, Hudson CS, Agre P, Nielsen S. Direct immunogold labeling of aquaporin-4 in square arrays of astrocyte and ependymocyte plasma membranes in rat brain and spinal cord. *Proc Natl Acad Sci U S A*. 1998;95:11981-11986

31. Tomas-Camardiel M, Venero JL, Herrera AJ, De Pablos RM, Pintor-Toro JA, Machado A, Cano J. Blood-brain barrier disruption highly induces aquaporin-4 mrna and protein in perivascular and parenchymal astrocytes: Protective effect by estradiol treatment in ovariectomized animals. *J Neurosci Res*. 2005;80:235-246

32. Ito H, Yamamoto N, Arima H, Hirate H, Morishima T, Umenishi F, Tada T, Asai K, Katsuya H, Sobue K. Interleukin-1beta induces the expression of aquaporin-4 through a nuclear factor-kappab pathway in rat astrocytes. *J Neurochem*. 2006;99:107-118

33. Nicchia GP, Nico B, Camassa LM, Mola MG, Loh N, Dermietzel R, Spray DC, Svelto M, Frigeri A. The role of aquaporin-4 in the blood-brain barrier development and integrity: Studies in animal and cell culture models. *Neuroscience*. 2004;129:935-945

34. Simard JM, Kent TA, Chen M, Tarasov KV, Gerzanich V. Brain oedema in focal ischaemia: Molecular pathophysiology and theoretical implications. *Lancet Neurol*. 2007;6:258-268

35. Quick AM, Cipolla MJ. Pregnancy-induced up-regulation of aquaporin-4 protein in brain and its role in eclampsia. *Faseb J*. 2005;19:170-175

36. Jeyaseelan K, Lim KY, Armugam A. Microrna expression in the blood and brain of rats subjected to transient focal ischemia by middle cerebral artery occlusion. *Stroke*. 2008;39:959-966

37. Kamsteeg EJ, Hendriks G, Boone M, Konings IB, Oorschot V, van der Sluijs P, Klumperman J, Deen PM. Short-chain ubiquitination mediates the regulated endocytosis of the aquaporin-2 water channel. *Proc Natl Acad Sci U S A*. 2006;103:18344-18349

38.   Carmosino M, Procino G, Nicchia GP, Mannucci R, Verbavatz JM, Gobin R, Svelto M, Valenti G. Histamine treatment induces rearrangements of orthogonal arrays of particles (oaps) in human aqp4-expressing gastric cells. *J Cell Biol*. 2001;154:1235-1243
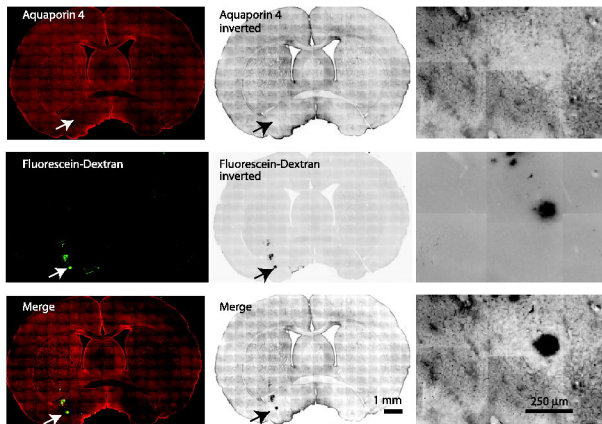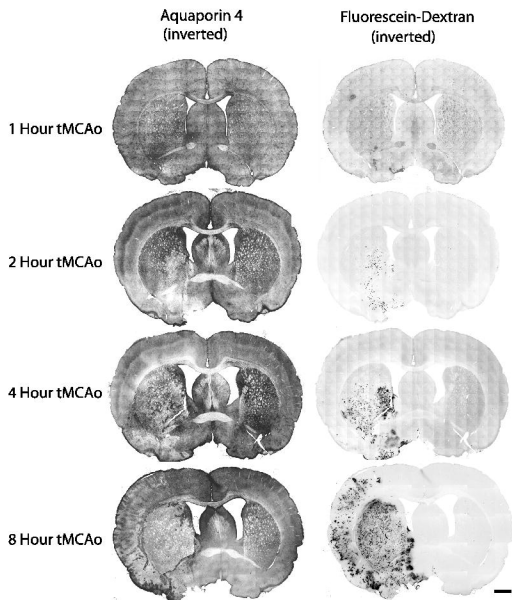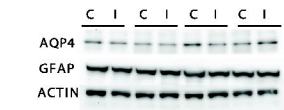
One Hour tMCAo

Aquaporin 4

Aquaporin 4
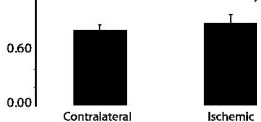inverted

Fluorescein-Dextran

Fluorescein-Dextran
inverted

Merge

Merge

1 mm

250 μm

Figure 1
Friedman et al.

	Aquaporin 4 (inverted)	Fluorescein-Dextran (inverted)
1 Hour tMCAo		
2 Hour tMCAo		
4 Hour tMCAo		
8 Hour tMCAo		

Figure 2
Friedman et al.

A. 8 Hour tMCAo Protein

C I C I C I C I

AQP4

GFAP

ACTIN

Striatum GFAP: Normalized Denistometry

1.20

0.60

0.00

Contralateral   Ischemic

Striatum AQP4: Normalized Denistometry

1.20

0.60

0.00

Contralateral   Ischemic

B. 8 Hour tMCAo mRNA

GFAP mRNA

5.0
4.0
3.0
2.0
1.0
0.0

** **

AQP4 mRNA

1.5

1.0

0.5

0.0

ns   ns

Contralateral   Cortex   Striatum
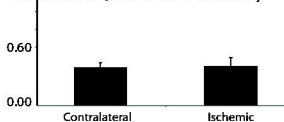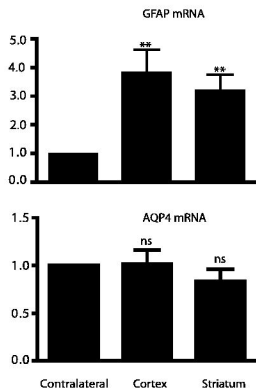
C. 8 Hour tMCAo Striatal Microvessels

C1   AQP4
      Dextran

C2   X-Z

10 μm   10 μm

C3   C4   X-Z
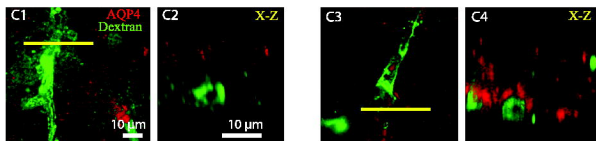
Figure 3
Friedman et al.

A. Laser Scanning Cytometry
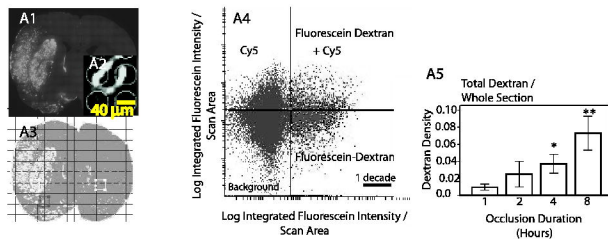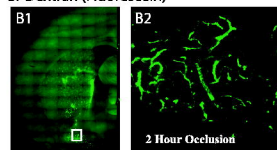
A1

A2

40 μm

A3

A4

Cy5   Fluorescein Dextran + Cy5

Log Integrated Fluorescein Intensity / Scan Area

Background   Fluorescein-Dextran

1 decade

Log Integrated Fluorescein Intensity / Scan Area

A5   Total Dextran / Whole Section

Dextran Density

Occlusion Duration (Hours)

B. Dextran (Fluorescein)

B1

B2   2 Hour Occlusion

C. Dextran+ AQP4 (Cy5)

C1

C2

D. Dextran+ IgG (Cy5)

D1

D2

E. Dextran+GFAP (Cy5)

E1

E2

1 mm   100 μm

F. Whole Section Double-Labeling

AQP4-Dextran/ Total Dextran

Double Label Index

IgG -Dextran/ Total Dextran

Occlusion Duration (Hours)

GFAP-Dextran/ Total Dextran
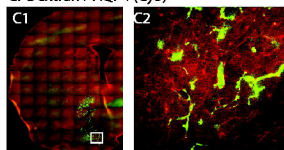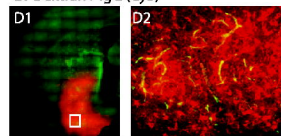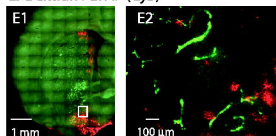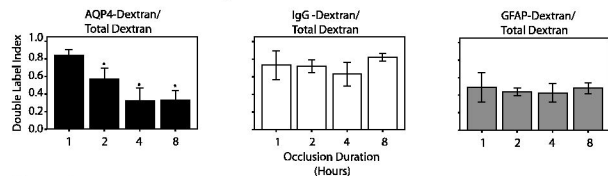
Figure 4
Friedman et al.

A.

AQP4
High vs Low Dextran Subregions
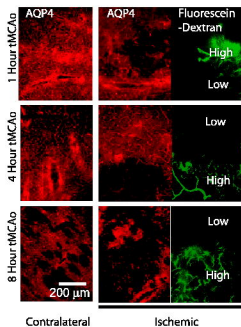
B.

Dextran Density
High vs Low Dextran Subregions

C.

AQP4
High vs Low Dextran Subregions

Occlusion Duration
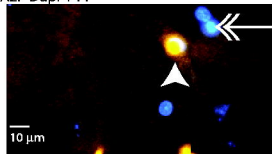(Hours)

Figure 5
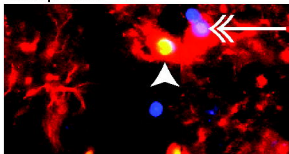**Friedman et al.**
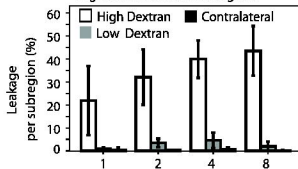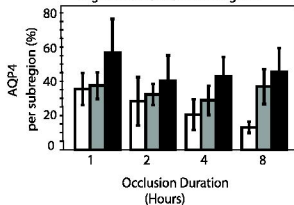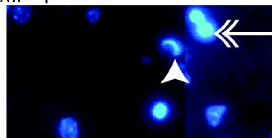
A1. Dapi Positive

B1. Dapi + GFAP

A2. Dapi + Pi

10 μm
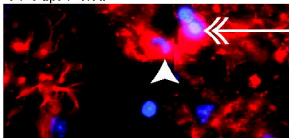
B2. Dapi + GFAP + Pi

C. Proportion of Dapi + GFAP +Pi

■ Dapi Positive
■ Dapi + Pi
□ Dapi + GFAP

■ Dapi +Pi
□ Dapi + GFAP + Pi

Number of Labeled Cells

1548   120
        170

170   31

Figure 6
Friedman et al.